Journal of Materials Processing Technology 209 (2009) 6124–6133

Contents lists available at ScienceDirect

Journal of Materials Processing Technology

journal homepage: www.elsevier.com/locate/jmatprotec

Computer simulation of the two-body abrasion process modeling the particle as a paraboloid of revolution

Liang Fang[a,b,*], Bo Li[a], Jia Zhao[a], Kun Sun[a]

[a] The State Key Laboratory for Mechanical Behavior of Materials, Xian Jiaotong University, Xian 710049, PR China
[b] School of Materials, Science and Engineering, China University of Mining and Technology, Xuzhou 710055, Jiangsu Province, PR China

ARTICLE INFO

Keywords:
Two-body abrasion
FEM
Monte Carlo method
Revolution parabolic particles

ABSTRACT

Two-body abrasive wear is a process with strong stochastic characteristic. Abrasive particle geometry, distribution and worn surface morphology can only be statistically determined and analytical models therefore always cause large inaccuracy. In this research, the earlier model of a particle as pyramid with a hemispherical tip has been replaced by a paraboloid model of revolution. In the pyramid model the normal load cannot be large enough to penetrate beyond the height of the hemisphere. Generally, in practice the hemisphere tip is quite small, and it readily penetrates into the surface. A new particle model has, therefore, been devised to extend the normal load range. New contact equations are proposed for the particle geometry used in the present model. The Monte Carlo method and finite element methods (FEMs) have also been combined to calculate the wear rate of the material during simulation. It is found that the linear wear rate increases continuously during the running-in process and reaches a constant value after some travel distance. Computed roughness and worn surface morphologies are in agreement with the experimental data. Finally, a comparison between simulated and experimented wear rates has also made. Both data matched very well.

1. Introduction

Two-body abrasion is a process during which hard particles or asperities cause matched surface damages during relative sliding. The two-body abrasion process should be considered as a stochastic process because of abrasive particle shapes and their statistical distributions relative to the matched surface with a strong statistical behavior. Furthermore, the worn surfaces also exhibit strong statistical characteristics because of sochastic positions acted on surface by particles. The classical mathematical models usually cannot easily predict the wear rate of worn materials. Some models predict a wear rate of materials at least one order of magnitude larger than the experimentally observed values. In order to properly describe the two-body abrasion process, a stochastic process should be introduced. Some researchers have made successful attempts using stochastic models. Some researchers (Zhang and Xie, 1989a,b,c) have proposed surface roughness stochastic model of two-body pure microcutting wear and Nicholls and Stephenson (1995) proposed a Monte Carlo model of erosion processes which is effective.

A random generator of computer has been taken to establish a statistical model of two-body abrasion (Jacobson et al., 1987). The model is successful in qualitatively predicting the influence of wear parameters on wear rate, such as grit size, load and material hardness. However, careful comparison of the simulation results with experimental values shows that the wear rates differ from one order of magnitude. The reason is from parameters of groove ridges pushed aside by abrasive particle that have not been directly introduced and a pure microcutting mechanism is considered. Besides a constant cone angle with a constant tip radius of abrasive particles is also assumed instead of random parameters. Jiang et al. (1998) have proposed an assumption of conical particles with round tips similar to Jacobson's particle model. In that model, the groove ridge is considered. The experimental data of Hokirigawa and Kato (1989) are used to estimate the removal fraction of material from the groove. A wear rate is with the same order of magnitude compared to the experimental values. However, random parameters of particle geometry have not yet been introduced although the tip radius and apex angle of particles are set as real variables.

In our previous work (Fang et al., 2005), a stochastic process is proposed considering abrasive particle shapes and their distribution with stochastic parameters. Furthermore, the decreases of wear volume due to groove ridges pushed aside by abrasive particle are also taken into account in the model. The simulated and experimented data matched very well. However, it has been noticed that the defined normal load cannot be large enough to penetrate beyond the height of semisphere for a pyramid model. For a practical case, it is necessary to expand normal load range.

* Corresponding author at: The State Key Laboratory for Mechanical Behavior of Materials, Xian Jiaotong University, Xian 710049, PR China.
E-mail address: fangl@xjtu.edu.cn (L. Fang).

0924-0136/$ – see front matter © 2009 Elsevier B.V. All rights reserved.
doi:10.1016/j.jmatprotec.2009.04.017

Nomenclature

a	x-coordinate distance from axes for parabolic grit
A	pile-up height of groove
A_g	area of groove
A_a	area of right ridge
A_b	area of left ridge
A_e	elastic contact area
A_{ep}	elastoplastic contact area
A_p	plastic contact area
A_1, A_2, A_3	different constants individually, related to material properties
$B_1 B_2 B_3$	constants unrelated to material properties
D	grit diameter of conical shape grit
f_{ab}	factor of the wear
h	height of a parabolic asperity
h_c	average height of surface
H_f	frustum height for conical grit with a semispherical tip
H_g	height of grit for conical shape with a semispherical tip
k	coefficient for Azarkhin and Böklen's curves of ridge
k_1, k_2, k_3, k_4, k_5	constants related to material properties
l_{step}	length of per grooving step
n_x, n_y	subdivided points numbers in x and y directions
P_{me}	the maximum elastic contact pressure
P_{ae}	mean elastic contact pressure
P_e	elastic contact load
P_{aep}	mean elastoplastic contact pressure
P_{ep}	elastoplastic contact load
P_p	plastic contact load
r	grit radius at the bottom for parabolic grit
r_0	half width of the groove
r_s	tip radius for conical grit with a semispherical tip
R	elastic contact of a flat with a sphere of radius
w	z-coordinate distance from axes in parabolic grit
w_e	elastic contact load of an asperity
w_p	plastic contact load of an asperity
W	pile-up width
x_c	constant related to the apex of asperity
y	coordinate of ridge's height
z	coordinate of ridge's height
z_0	average height of all the mesh unit before the first grooving step
$z_{i,j}$	z-coordinate for the mesh unit $[i,j]$ at the Nth sliding step
θ	apex angle of the conical shape grit

In the present research, a revolution parabolic particle geometry is applied to improve the earlier model of pyramid with semisphere tip, so much the shortcoming of penetrating particle tip can be thrown away. In the present work relative contact equations are also proposed to match the new particle geometry. Monte Carlo shooting method and finite elements method (FEM) are combined together to calculate the wear rate of material during simulation.

2. Parabolic particle model

A statistical approach derived from the observation to common engineering surfaces produced by standard machining process (e.g. ground surfaces) are characterized by a random topography from the work of Greenwood and Williamson (1966). The surface asperities are often simulated with many hemispheres assuming for the asperity heights opportune distribution functions (e.g. Gaussian one). In that way it becomes easy to obtain simple equations that allow fast contact analyses. However, the exactitude is strongly dependent on the assumption on asperity shape and heights distribution.

Although Greenwood and Williamson (GW) model has been widely used to describe the asperity contacts, the necessary input data, such as, summit asperity height deviation, mean radius and asperity density cannot be easily got by usual commercial profilometers. A numerical procedure to calculate the input data of GW model is, therefore, proposed (Tomanik et al., 2003) and an extension of Nayak's theory to elliptic model of rough surface contacts is also given (Greenwood, 2006). A few works report the effect that sliding contact on the stress for a spherical contact (Nicholls and Stephenson, 1995). Many have also focused on the adhesion between a sphere and a flat rather than the sliding interaction between two spheres (Jacobson et al., 1987).

However, the diameter of hemisphere is quite small in the real world. It is easily penetrated beyond the height of hemisphere. In the pyramid model a normal load cannot be too large to penetrate beyond the height of hemisphere. Therefore, it is necessary to construct a new particle model to expand normal load range. In this research, revolution parabolic particle geometry is applied to improve the earlier model of pyramid with hemisphere tip.

In the report by Aramaki et al. (1993), a model of roughness description is proposed to represent the measured rough profile with quadratic functions. That model, based on the parabolic indenter in elasticity, calculates the average pressure and the real contact area in a contact between two longitudinally rough surfaces. Every asperity is represented as a parabola with width L defined as the distance between two points at which the real asperity crosses a reference plane (Fig. 1).

The analytical simulation of the surface morphology makes it easy to determine key roughness parameters, such as, peaks curvature, summit and width, that can be used for solving contact problems. Five different models are presented and applied to five profiles obtained by profilometric analysis of some very different specimens used in dry and lubricated tests that had undergone some running-in or even wear (Ciulli et al., 2008). The simulation of parabolic surface morphology gives the better approximation of profiles.

In our earlier work, the computer simulation of two-body abrasion process, all grits are assumed to be of conical shapes with round tips (as shown in Fig. 2). They are randomly distributed in the abrasive surface. In the model, the position distribution of grits is considered to be uniform in the abrasive surface. The relation of geometrical parameters of grits can be described as

$$\begin{cases} D - 2r_s \cos\theta = 2H_f \tan\theta \\ H_g = H_f + r_s(1 - \sin\theta) \end{cases} \quad (1)$$

where H_f is the height of grits frustum, D is the grit diameter, H_g is the grit height, r_s is the tip radius and θ is the apex angle. In the above

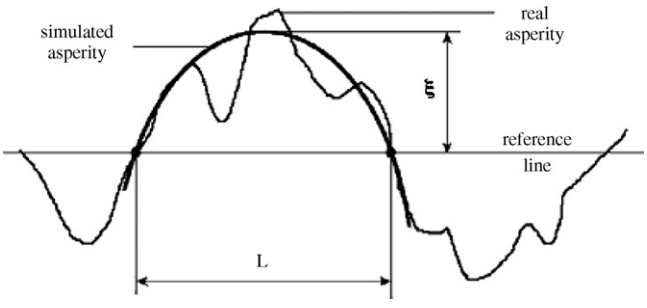

Fig. 1. Schematic of an asperity approximation (Aramaki et al., 1993).

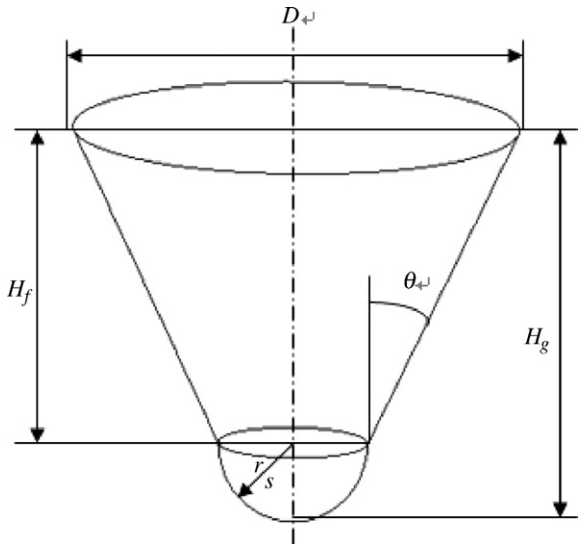

Fig. 2. Grit in conical shape with hemispherical tip.

equation, there are only three independent variables. Therefore, D and H_g are assumed to follow a Gaussian normal distribution. The tip radius r_s is assumed to have a uniform distribution. The distribution of the apex angle θ and the frustum height H_f are dependent upon other variables and their distributions as shown in Eq. (1). To produce a random grit surface, a Monte Carlo shooting method is used. The vacancies can be sought automatically during planting grits. Using that method, a quite uniform grit surface can be satisfactorily produced.

As mentioned before, it is necessary to construct a new particle model to expand normal load range. In this research, revolution parabolic particle geometry is applied to improve the earlier model of pyramid with semisphere tip as shown in Fig. 3. The relation of geometrical parameters of grits can be described as

$$w = \frac{h}{r^2} \cdot a^2 \tag{2}$$

where h is the grit height, r is the grit radius, w is the z-coordinate distance from axes and a is the x-coordinate distance from axes.

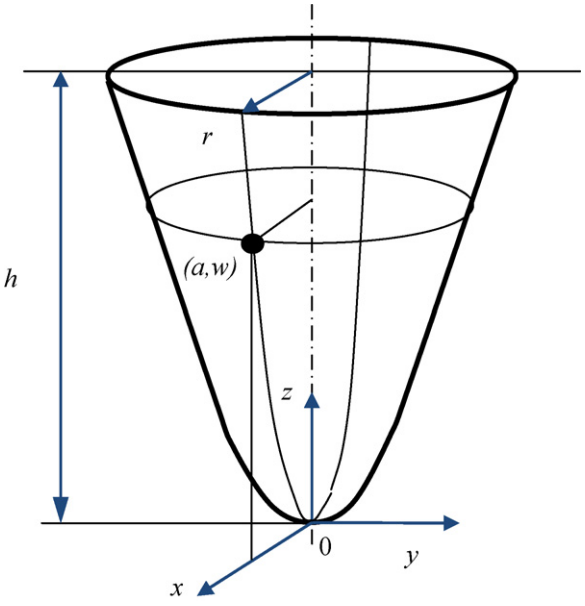

Fig. 3. A grit in parabolic shape.

There are only two independent variables compared to Eq. (1). Therefore, r and h are assumed to follow a Gaussian normal distribution. The tip radius r which is assumed to have a uniform distribution has been deleted in the new particle model. Then, a shooting method is used to produce a random uniform grit surface.

The new particle model gives an influence on the rough profiles by parabola functions obtained using simple parameters of roughness. Parabolas have been used for describing the peaks and the valleys in literatures. A distinguish for different parabola particle is defined by each consecutive couple of points where the measured profile crosses the reference line and the corresponding heights are equal to zero. The mathematical expression of profile for one particle can be described as follows:

$$y = a_1x^2 + a_2x^4 + a_3x^6 + \dots \tag{3}$$

3. Contact mechanics

New contact mechanics equations are necessary to match the revolution parabolic particle. The pioneering contribution to this is made by Greenwood and Williamson (1966), who developed a basic elastic contact model (GW model). In their model, a rough surface is represented by a population of hemispherical tip asperities of identical radius of curvature with their height following a Gaussian distribution. The basic asperity in GW model has been extended to other contact geometries based on contact-mechanics theories in conjunction with the continuity and smoothness of variables across different modes of deformation. Three deformation stages are studied individually by former works. The load is calculated as a function of the interference of each profile with a rigid smooth flat surface for single parabolic asperities.

3.1. Comparison between hemisphere tip and parabolic tip

Consider the contact between one hemisphere asperity and a smooth flat at first. Let a and R stand for the radii of the sphere knocked in and the radii of the hemisphere, respectively. Then, w is the contact interference. The equation is established as follows:

$$a^2 = R^2 - (R - w)^2 = 2Rw - w^2 \tag{4}$$

The interference w is an important variable that measures the extent of the asperity deformation. The contact pressure and contact area of the asperity are fully determined by this interference. According to the Hertz theory for the elastic contact of a flat, the elastic deformation of asperity is sufficiently small, as $R \gg w$. Thus, Eq. (4) is rewritten to give

$$a^2 = 2Rw \tag{5}$$

Then consider the contact between a parabolic tip asperity with a smooth flat. The function of a parabolic profile is given as

$$w = \frac{h}{r^2} \cdot a^2 \tag{6}$$

where h is the height of a parabolic asperity, r is the radii at the bottom of a particle. As w stands for the same contact interference in Eqs. (5) and (6), the following expression is obtained for R, r and h:

$$R = \frac{r^2}{2h} \tag{7}$$

3.2. Contact of a single parabolic asperity with a smooth surface

The asperity will experience three distinct deformation stages as w increases: elastic, elastic–plastic and fully plastic. The distinct deformation stages can be divided by the elastic contact load of an asperity w_e and the plastic contact load of an asperity w_p. The

following sections develop formulations for the mean contact pressure and real area of contact of the asperity as functions of w during the three deformation stages.

(1) Elastic contact ($w < w_e$). The asperity deforms elastically when w is sufficiently small. According to the Hertz theory for the elastic contact of a flat with a sphere of radius R, the contact area A_e, contact load w_e, the maximum contact pressure P_{me}, average contact pressure P_{ae} and mean contact pressure P_e of the asperity can be expressed in terms of w as

$$A_e = \pi \cdot w \cdot \frac{r^2}{2h} \tag{8}$$

$$P_e = \frac{4}{3}E^* w^{3/2}\left(\frac{r^2}{2h}\right)^{1/2} \tag{9}$$

$$P_{me} = \frac{2E^*}{\pi}\left(\frac{2wh}{r^2}\right)^{1/2} \tag{10}$$

$$p_{ae} = \frac{2}{3}p_{me} = \frac{4E^*}{3\pi}\left(\frac{2wh}{r^2}\right)^{1/2} \tag{11}$$

It is shown by Tabor (1951) that, when the maximum Hertz contact pressure reaches $P_{mc} = 0.6H$, or, the average contact pressure $P_{ae} = 0.4H$, the initial yielding occurs. For a more general form the mean contact pressure P_{ae} can be correlated at the point of initial yielding with the hardness by

$$P_{ae} = kH \tag{12}$$

The critical interference, w_e, at the point of initial yielding can be expressed in terms of the parameters of the contacts. Eq. (11) is rewritten to give

$$w = \left(\frac{3\pi P_{ae}}{4E^*}\right) \cdot \frac{r^2}{2h} \tag{13}$$

Then, substituting Eq. (12) into Eq. (13), yields

$$w = \left(\frac{3\pi kH}{4E^*}\right)^2 \cdot \frac{r^2}{2h} \tag{14}$$

When $w < w_e$, the contact is elastic. When $w \geq w_e$, the contact is either elastoplastic or fully plastic.

(2) Elastoplastic contact ($w_e < w < w_p$). Based on Johnson's work (Johnson, 1985), fully plastic deformation occurs when P_e, is about equal to 400 times that at initial yielding, P_p, or

$$\frac{P_e}{P_p} = 400 \tag{15}$$

Using Eq. (9), which is valid for elastic contact, the following expressions are obtained for P_p

$$P_p \leq \frac{4}{3}E^* w_p^{3/2}\left(\frac{r^2}{2h}\right)^{1/2} \tag{16}$$

By substituting the above Eq. (9), Eq. (15) and Eq. (16), the following expression is obtained

$$w_p \geq 54 w_e \tag{17}$$

According to the ZMC model (Zhao et al., 2000) the contact area A_{ep}, mean contact pressure P_{aep} and elastoplastic contact load of an asperity P_{ep} are given by

$$A_{ep} = \pi w \cdot \frac{r^2}{2h} \cdot \left[1 - 2 \times \left(\frac{w - w_e}{w_p - w_e}\right)^3 + 3 \times \left(\frac{w - w_e}{w_p - w_e}\right)^2\right] \tag{18}$$

$$P_{aep} = H - H \cdot (1 - k) \cdot \frac{\ln w_p - \ln w}{\ln w_p - \ln w_e} \tag{19}$$

$$P_{ep} = P_{aep} \times A_{ep} \tag{20}$$

(3) Fully plastic contact ($w > w_p$). When w is increased to another critical value w_p at which the mean contact pressure P_{ep} of the asperity reaches the value of H, fully plastic deformation occurs. During the stage of fully plastic deformation, the mean contact pressure P_{ep} remains constant at H, or

$$P_{ep} = H \tag{21}$$

The contact area, according to Abbott and Firestone (1933), is equal to the geometrical intersection of the flat with the original underformed profile of the asperity, or

$$A_p = \int_0^w 2\pi \cdot a \cdot dw = \frac{4}{3}\pi\left(\frac{r^2}{h}\right)^{1/2} w^{3/2} \tag{22}$$

where a is described as

$$a = \left(\frac{r^2}{h} \cdot w\right)^{1/2} \tag{23}$$

The contact load P_p of the asperity is equal to the contact area multiplied by the mean contact pressure, or

$$P_p = A_p \cdot P_{ap} = \frac{4}{3}\pi \cdot w^{3/2} \cdot \left(\frac{r^2}{h}\right)^{1/2} \cdot H \tag{24}$$

Based on the Hertz theory of elastic contact for a flat with a sphere, the present work is satisfied with the inequality $r^2/2h \gg w$. When w increases over the critical value, the fully plastic average contact pressure, or the hardness, varies with the deformed contact geometry.

4. Ridge morphological curves determination

Two-body abrasion is a typical wear pattern. During this process, a plastic deformation behavior of worn material has a strong effect on the wear procedure. The volume loss caused by a single grit can be determined by

$$f_{ab} = \frac{A_g - (A_a + A_b)}{A_g} \tag{25}$$

It becomes clear that the quantity estimation for plastic ridges distributed on both sides of groove is quite difficult, therefore, many previous wear models do not include that parameter. This results in overrating of the wear volume of worn material. Kayaba et al. (1986), and Hokkirigawa and Kato (1988) noticed, from in situ SEM observations of scratching surface by hemisphere grit, that wear pattern will change to cutting mode ($f_{ab} \approx 1$) from ploughing mode ($f_{ab} = 0$) and ridge-forming mode ($0 < f_{ab} < 1$) with varying indentation depth. In accordance with the wear mode change, the volume fraction of ridge to groove also varies greatly so as to bring about a large change of wear amount.

Azarkhin (Azarkhin and Richmond, 1992) uses upper bound approach to build a relationship of ridge geometrical parameters to friction coefficient using a rigid pyramid tip scratching over rigid-plastic material. Böklin (1973) carried out a normal indentation test by a hard cone. Curves of ridge can be approximately described as parabolic type:

$$z = -\frac{4A}{W}(x - k)^2 + W \tag{26}$$

where z is the coordinates of ridge's height, A is the pile-up height, W is the pile-up width and k is a constant. Its value is determined by ridge's positions that are at the right or left side of the groove.

It is evident that test material and contact model both have predominant influences on the ridge geometrical parameter and upper bound approach is also quite weak to simulate real scratch test. Those results are, therefore, not adequate for the purpose of simulation.

Because the exact measurement of ridge geometrical parameters is uneasy and tedious after scratching, the implementation of computer simulation is desirable. With new improvements of computation capability and commercial software of finite elements method, three-dimensional FE computations with huge number of nodes have become faster with a conventional personal computer. Therefore, three-dimensional finite element method analysis is used in this investigation. Stress and strain of a half infinite plane indented by a sliding sphere tip are calculated with an elastic-linear strengthen plastic deformation model by commercial software. The curves proposed by Azarkhin and Böklen are modified by the FEM calculation. The expression of fitting curve for ridge is given by the present authors (Fang et al., 2005):

$$y = \left[k_0 + \left(\frac{2k_1}{\pi}\right) \times \frac{k_2}{4 \times (D_p \times W - k_3)^2 + {k_2}^2}\right] \times [x - (k_4 \times D_p \times W + k_5)]^3$$

where k_1, k_2, k_3, k_4 and k_5 are different constants individually, related to material properties.

In the Monte Carlo simulation process, the discrete coordinate values of ridge contour should be transformed into continuous curve to overlap new curve to the worn surface curve. Therefore, fitting treatment is necessary in this research. According to literature (Fang et al., 2005), five constants in the fitting curve of ridge expressed above have insubstantial physical meanings. Moreover, the expression of fitting curve of ridge varies a lot as the interference of an asperity changes. However, during the two-body abrasion process, it is considered as a stochastic process because of abrasive particle shapes and their statistical distributions relative to the matched surface. Thus, it is difficult for computer simulation of two-body abrasion processes to finish with asperities of statistical hemisphere radii. The present work is to give a new expression of fitting curve of ridge with constants of substantial meanings as Böklen obtained. Also, the expression is based on results of FEM calculation. In Cartesian coordinate system, the fitting curve of ridge can be rewritten as follows

$$y = A\,e^{(-e^{(-z)}-z+1)} \tag{27}$$

and

$$\begin{aligned} z &= x - x_c \\ x_c &= A_1 + B_1 r_0 \\ W &= A_2 + B_2 r_0 \\ A &= A_3 + B_3 r_0 \end{aligned} \tag{28}$$

where y is the coordinates of ridge's height, r_0 is the half of the furrow, A is the pile-up height, W is the pile-up width and x_c is a constant related to the apex of a asperity. A_1, A_2 and A_3, are different constants individually, related to material properties, but B_1, B_2 and B_3 are constant unrelated to material properties. New expressions of the fitting curve of ridge have similar parameters with Böklen's curve. The discrete coordinate values of ridge contour can be transformed continuously as the interference increases in the computer simulation of two-body abrasion process.

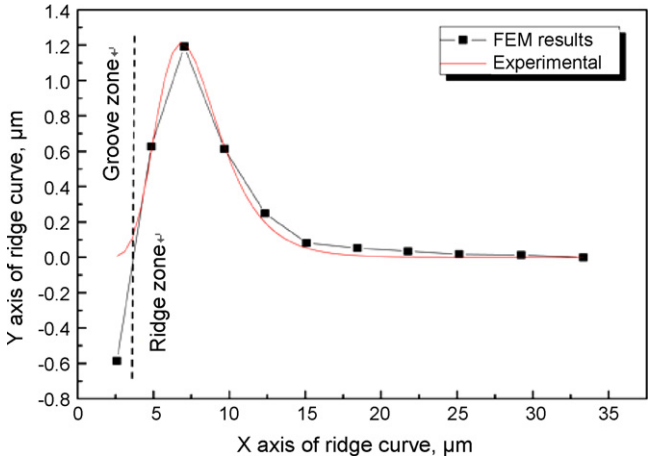

Fig. 4. New expressions of the fitting curve.

After the dot of zero height nearby the groove is set as the origin of coordinates, the effect of material hardness on ridge curve pattern can be clearly investigated by the new curve. Fig. 4 shows the regressive fitted curves of ridge for AISI1080 steels in the indented depth of 0.04 mm. From Fig. 4, it can be seen that much smaller tolerance is obtained by the new fitting curve of ridge related to the FEM results, compared to earlier approach. More accurate f_{ab} factor is brought in computer simulation at present which leads to the better results calculated by computer simulation.

5. Experiments and results

5.1. Computer simulation process

5.1.1. Simulation parameters

The simulation parameters of the abrasive paper are chosen from Jacobson et al. (1987). It is shown in Table 1. The parameters of the simulated steels are listed in Table 1. In two-body abrasion tests, SiC abrasive paper with various average diameters is used. Their mechanical properties are also shown in Table 1.

To match the data of Table 1 showing the simulation parameters, different average sizes of SiC abrasive papers are chosen in the wear tests to compare simulation results with the experimental results. Before starting the simulation, a 200 mm × 10 mm abrasive belt is produced by Monte Carlo method based on previous work (Fang et al., 2005). In Monte Carlo method grit size is assumed to obey Gauss distribution and grit position uniform distribution, seperately. In a designed abrasive belt surface grits are randomly and evenly "planted" on the surface one by one using the computing algorithm of a shooting method to avoid grits overlapping on the defined surface. The vacancies can be sought automatically during planting grits, and a quite uniform grit surface is satisfactorily produced as shown in Fig. 5. The sliding direction length is defined as 200 mm in this simulation. Mesh subdivision size is determined by average abrasive particle diameter. In the grooving direction, the mesh size is generally 1/10 of particle size. In the direction of verti-

Table 1
Mechanical properties of tensile tests for AISI steels and abrasives (Jacobson et al., 1987).

Material	Density (ρ) (g cm^{-3})	Poisson ratio (ν)	Young's modulus (E) (GPa)	Hardening modulus (E_p) (MPa)	Yield stress (σ_Y) (MPa)
1020	7.87	0.29	204	711	209
1045	7.85	0.26	210	1178	422
1080	7.85	0.26	211	1537	997
SiC	3.1	0.14	410	–	–

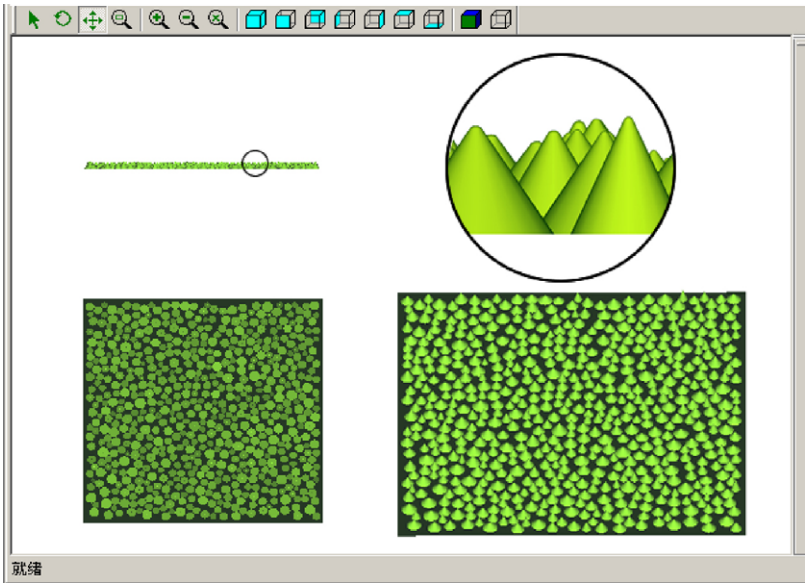

Fig. 5. Schematic of planted grit surface by computer.

cal grooving direction, the mesh size is chosen as 1/1000 of particle size. The simulated step size is 1×10^{-6} m. The simulated specimen is with 4 mm × 4 mm in size. The simulated wear data can be easily transformed to match with the experimental data with respect to equivalent normal pressure.

5.1.2. Calculating wear rate of materials

In order to accurately calculate the wear rate of materials and describe the worn surface roughness, the cubic column mesh unit is used in the present research. For each sliding step, the new-formed ridge curve is treated to be directly overlapped on the previous rough surface as to simplify the simulation process as mentioned in above section. Secondly, the grits move into depth range of material is ascertained, and their average height is accounted. Based on Johnson's contact model (Johnson, 1985) and ZMC model (Zhao et al., 2000), the contact load per particle is calculated. After obtaining the supported load per particle, the approach between the grits and the worn surface can be easily determined by an iteration approach. In the program the distance h_c between h_1 and h_2, which is the average height of surface, is iterated. Thus, the indented depths for related grits are determined. Fig. 6 shows the two-dimension schematic drawing of grits plate and specimen.

Hereto, the z-value of every mesh unit in the projected region of particle front side is estimated. Comparing the new z-value with the original z led to the determination of the volume loss of the corresponding mesh unit. The linear wear rate of all the mesh units after the Nth step's sliding can be calculated by

$$\varepsilon_L = \frac{z_0 - n_x^{-1} n_y^{-1} \sum_{i=1}^{n_x} \sum_{j=1}^{n_y} Z_{i,j}}{N l_{step}} \tag{29}$$

where z_0 represents the average height of all the mesh unit before the first sliding step and $z_{i,j}$ is the z coordinate values for the mesh unit $[i, j]$ at the Nth sliding step. Here, n_x and n_y are individually the subdivided points numbers in x and y directions. l_{step} is the length of per sliding step. All z-values on the specimen surface, therefore, define the morphology of worn surface after the Nth sliding step. The volume wear rate of the specimen can also be determined by multiplying the worn area by V_L.

In the present simulation, it is considered that the material removal fraction, that is, f_{ab}, by particle grooving, is mainly related to the mechanical properties of worn material, abrasive geometry and the supported load of grit. There is not any material removal criterion involved in the simulation. The material removal fraction can be got from a single grain contact calculation of FEM. The actual grooved surface geometry will not have directly contribution to the material removal fraction as it is mentioned that the new-formed ridge curve is treated directly to be overlapped on the previous surface.

It should also be mentioned here that in the FEM of groove ridge a linear strengthen material model with strain hardening capacity is applied. As compared to the strain hardening effects at the initial stage from early grain passages the succeeding strain hardening could be overlooked. That treatment will not give effects on the material removal because the material removal fraction, that is, f_{ab}, by previous grooving has been considered already from the previous FEM of groove ridge.

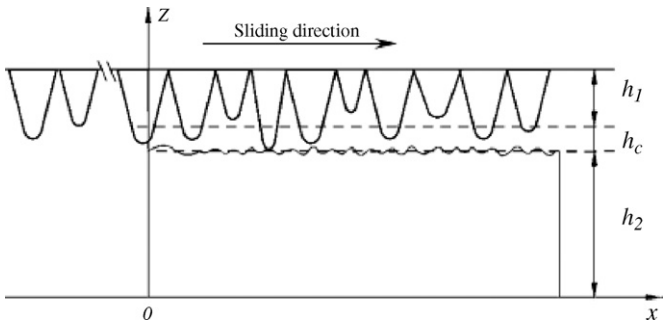

Fig. 6. Two-dimensional schematic drawing of grits plate and specimen.

5.2. Verifications of wear experiments

5.2.1. Roughness and worn surface morphology

Fig. 7 shows wear rate at each individual distance from the previous work by the present authors (Wu et al., 2000). It has been supposed that the linear wear rate was decreased continuously in running-in process and reached to a constant value after the running-in process. Khroschov (1966) found the running-in progress last for about 15 m long which is far larger than previous simulation progress.

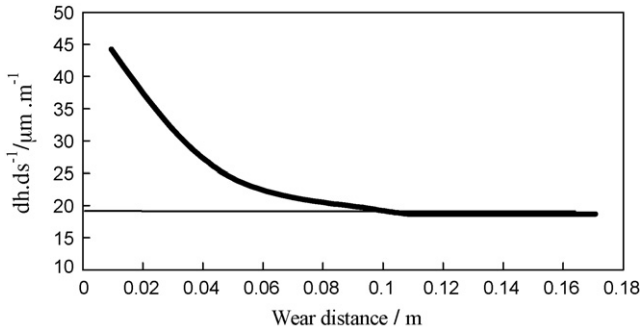

Fig. 7. Effect of sliding distance.

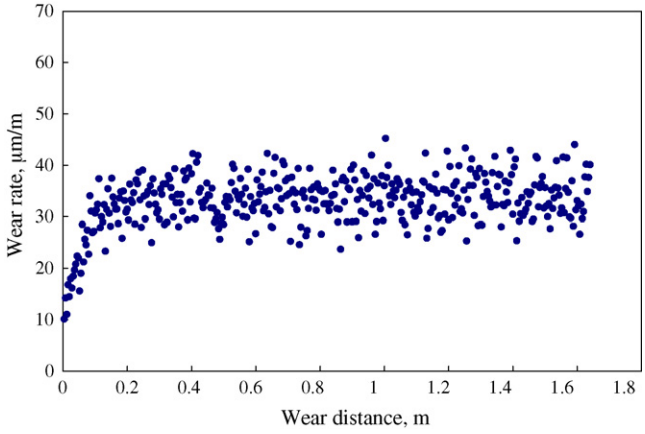

Fig. 8. Wear volume losses with travel distance.

The running-in progress in Fig. 7 finished merely within 0.12 m. Furthermore, the running-in progress occurred because of failure or clogging of abrasive grains under high-applied pressure (Khroschov, 1966), but such reason is neglected in the previous simulation (Wu et al., 2000). Thus, the continue decrease of linear wear rate in Fig. 7 cannot be supposed as a real running-in progress. Fig. 8 shows that the linear wear rate is increased rapidly at the initial stage within 50 steps which equals to 50 μm. It can be seen that wear rate has a linear increase at the beginning of the two-body abrasive process, then reaches a constant value after the running-in process. It is also seen from Fig. 8 that the simulative results of wear rates show strong statistic behavior at a certain range by several repeated calculations. When the simulation data in Fig. 8 are compared with that in Fig. 7, they are quite different. A few data at the very initial stage locate at running-in stage. Most data show a horizontal straight line distribution. The running-in stage in our case can be almost ignored because the breaking or clogging of abrasive grains under high-applied pressure has not been introduced in our simulation.

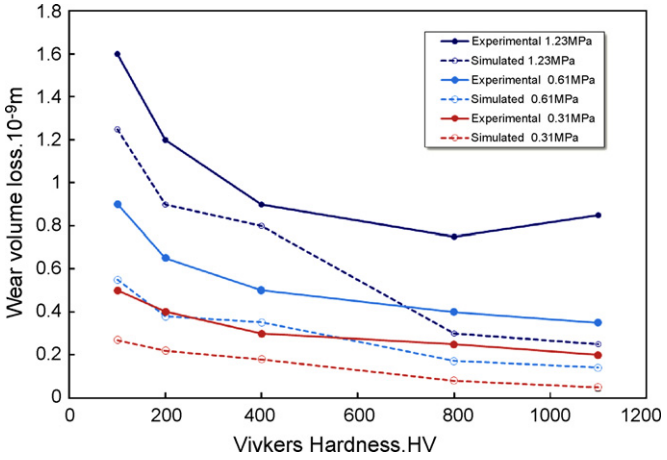

Fig. 10. Relationship between wear volume and Vickers hardness with apparent normal pressure 0.3, 0.61 and 1.23 MPa (Sasaki et al., 2006).

Accumulated wear rates related to simulation steps are shown in Fig. 9, where the several profiles of worn surface is also attached in which units for x coordinate is 4×10^{-8} m and units for y coordinate 1×10^{-6} m. It is indicated from the profile of worn surface that the initial stage ends before 30th steps and it can also be thought of there is almost no running-in stage.

5.2.2. Effect of hardness and normal pressure on wear rate

Hardness is an important monitor to abrasive wear. As a comparison the present authors introduce the abrasive wear tests on a pin-on-table test machine conducted by Umemoto et al. (2003) (Sasaki et al., 2006). In their tests the apparent applied pressures of the specimen with 0.31, 0.61 and 1.23 MPa, respectively, are applied against the Al_2O_3 abrasive paper with hardness about 2100 HV. Total wear distance is 5.0 m. Specimen materials are four steels with different cementite contents and pure iron, respectively. Fig. 10 shows the experimental curves of wear volume loss related to Vickers hardness using solid lines. It can be seen that the wear vol-

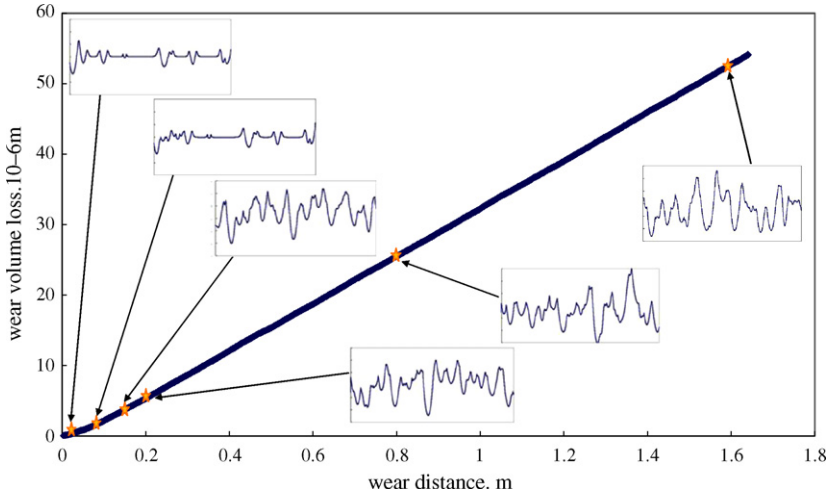

Fig. 9. Accumulated wear volume losses related to wear distance.

ume loss decreases with increasing Vickers hardness under every applied pressure.

The simulation is also correspondingly operated with the same experimental conditions. Fig. 10 shows the plots of wear volume loss V with respect to applied pressure P. Simulation results in Fig. 10 match the corresponding experimental results closely and exhibits slightly negative deviation. For pure iron (HV = 100) and S45C steel (HV = 200), V exhibits slightly negative deviation at an applied pressure of 1.23 MPa. However, the wear volume V which is simulated by computer is at about 50% less than the experimental value when the Vickers hardness is higher than 800 HV. This should be related to another wear mechanism, i.e., the fracture of cementite phase will be predominant with increasing volume fraction of cementite and higher normal pressure.

In Khruschov's tests (Khroschov, 1966) the wear resistance of different specimens of pure metal exhibits linear relationship as the related Brinell hardness grows up which has been shown in Fig. 11. The simulation is completed with the same experimental conditions correspondingly. Simulation results in Fig. 11 match the corresponding experimental results closely and also exhibits slightly negative deviation.

5.2.3. *Effect of grit size on wear rate*

The grit size has also a significant effect on the wear rate of materials besides hardness. It has been reported that there exists a critical size. Below that critical size, the wear rate increases with grit sizes, whereas above it the wear rate becomes unchanged with increasing abrasive sizes further as Khruschov reported (Khroschov, 1966). The present simulative results indicate that the wear amount increases linearly with increasing grit size. Especially, when grit size is bigger than 100 μm, the curve tends to be leveled off. The comparison of experimental data with the simulative results is shown in Fig. 12. It can be seen that the simulative results are lower than experimental data again. It is clear again that the results of the present model match with the experimental results very well.

5.2.4. *Roughness simulation and discussion*

To accomplish the Monte Carlo simulating, the average diameter of abrasive particles is defined as 138 μm and the parameters of abrasive paper are shown in Table 1. In that simulation, the mechanical properties of AISI1080 steel is also listed in Table 1. The size of the simulated specimen and related other parameters has also been mentioned in Section 5.1.1. Roughness curves are exhibited in Fig. 13 for some simulative steps. The simulated roughness Ra increases approximately linearly up to 3.13 μm for the first 20 steps and then keeps up and down that value. Here each individual step is 4 mm long and 20 steps equates to 0.8 m along the moving direction during simulation. In the wear test with the same conditions, AISI1080 steel is measured with the roughness Ra 3.22 μm. It can be noted that the final roughness of computer simulation progress exhibits slightly negative deviation and the error to experimental results is 2.8%. The simulation results fits well.

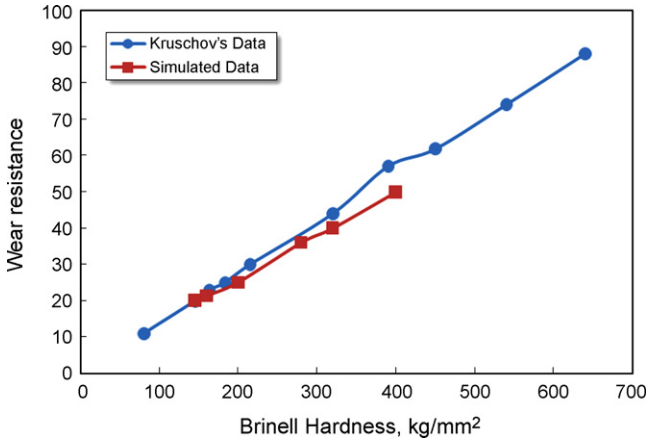

Fig. 11. Comparison of simulated results with varying metal hardness related to Khruschov test data (Khroschov, 1966).

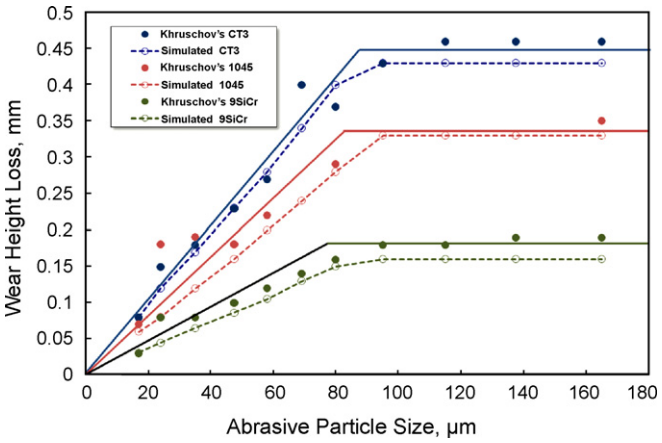

Fig. 12. Comparison of simulated results of three kinds of steel with varying grit size related to Khruschov test data (Khroschov, 1966).

5.2.5. *Worn surface morphology simulation*

The worn surface morphology of 5th, 10th, 30th, 50th, 200th and 400th steps is illustrated in Fig. 14 which shows the diversification of worn surface morphology from the 5th to 400th step. It can be seen that the wear is a gradual evolution process and after about 50th steps (50 μm) worn surface roughness turns to be a constant value as shown in Fig. 13 and most specimen surface has been touched by abrasive particles.

Worn surface morphology is obtained after abrasive wear test using AISI1080 steel as specimen as shown in Fig. 15. And the real three-dimension photograph of the AISI1080 for the same experiment is also measured by optical three-dimensional scanning profilometer as shows in Fig. 16. It can be seen that the main wear mechanism is grooving of abrasive particles. The simulation using the same parameters with two-body abrasive wear test is also carried out. The worn surface profile after the simulation is shown in Fig. 17. It is got by the comparison that the height of ridge and the depth of valley match the experimental profile very good. The difference is that the simulated worn surface of supposed specimen is flat and the real specimen surface is with a slight curve surface. The roughness between the experiment and simulation progress fits well which is mentioned above.

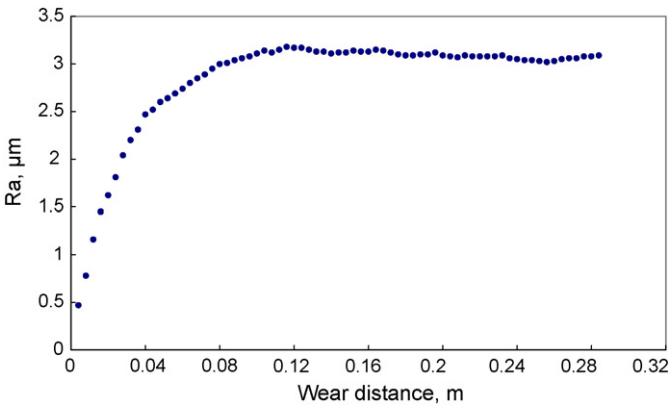

Fig. 13. Roughness at each individual step.

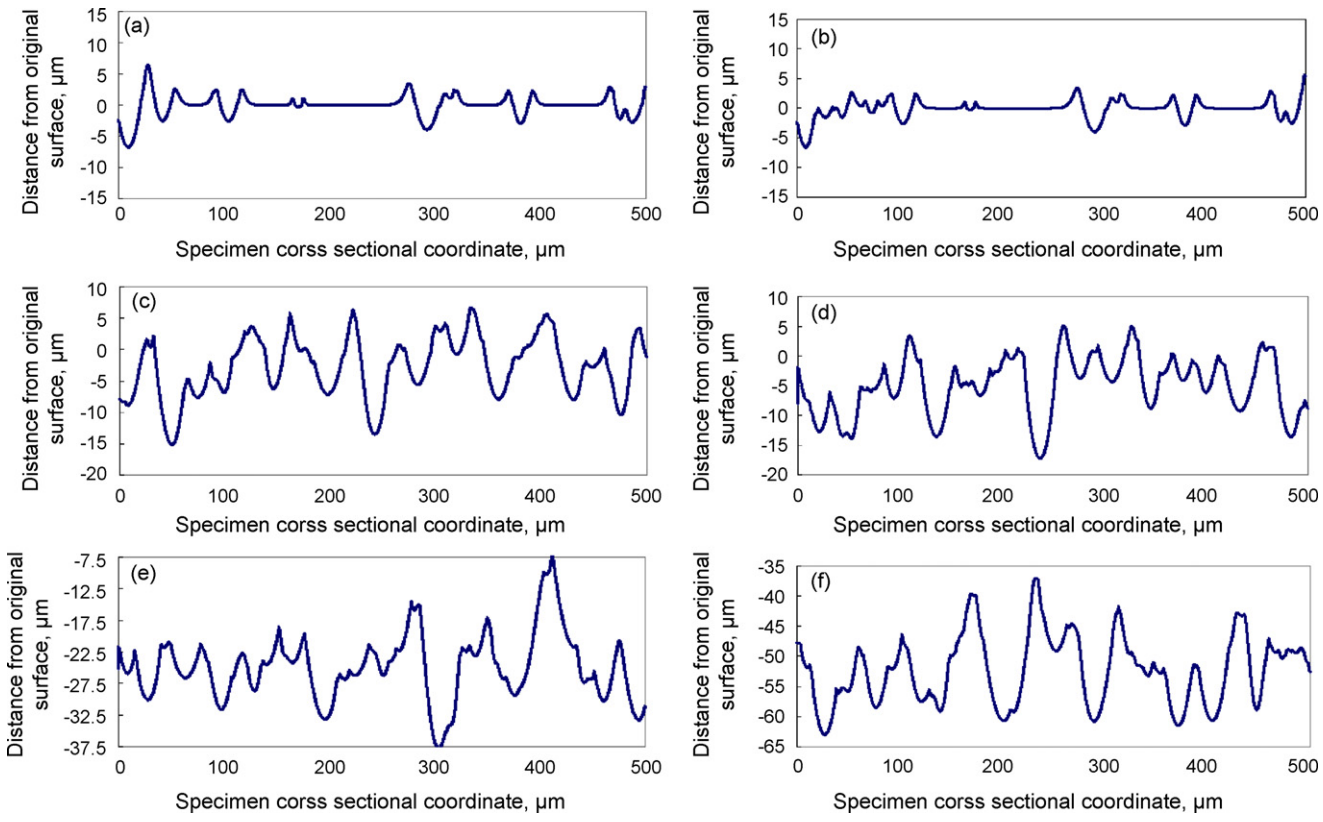

Fig. 14. Worn surface morphology of (a) 5th step, (b) 10th step, (c) 30th step, (d) 50th step, (e) 200th step and (f) 400th step simulation.

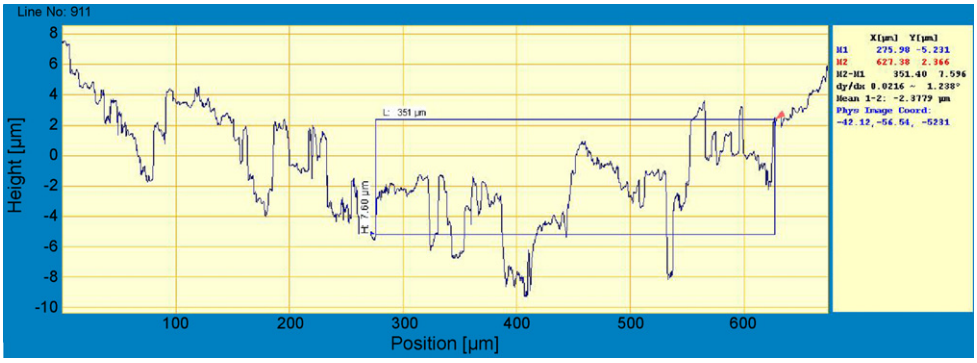

Fig. 15. Experimental worn surface profile of AISI1080 steel.

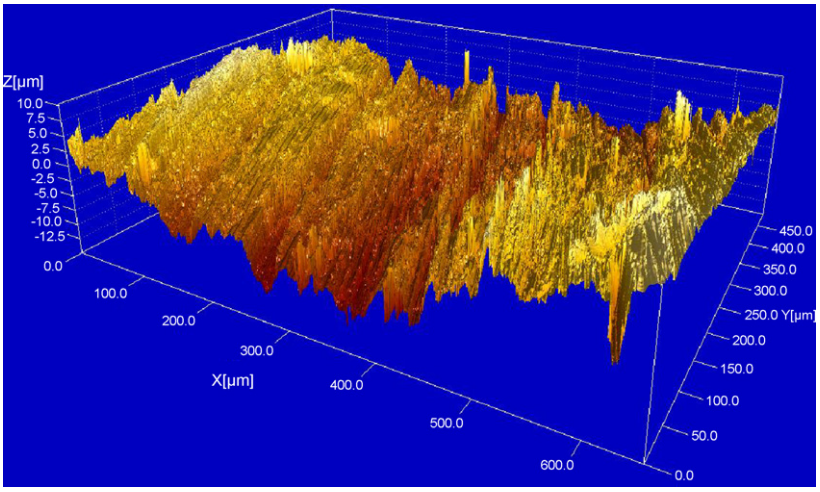

Fig. 16. Three-dimension photograph of AISI1080 steel.

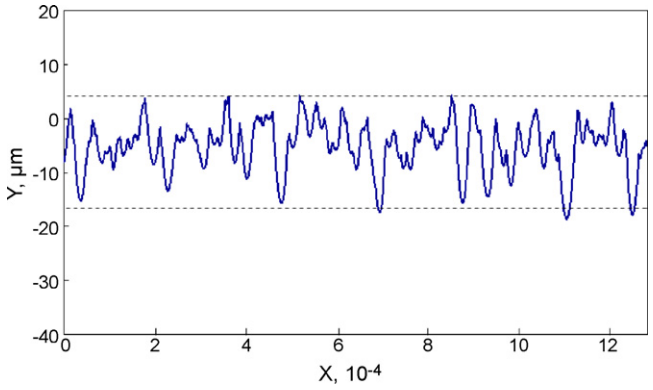

Fig. 17. Profile for simulation progress in the final step.

6. Conclusions

In this research revolution parabolic particle geometry is applied to improve the old model of pyramid with semisphere tip. In the pyramid model normal load cannot be large enough to penetrate beyond the defined height of semisphere. Generally, the diameter of semisphere is quite small in the real world. It is easily penetrated. Therefore, it is necessary to construct a new particle model to expand normal load range. The proposed particle models can describe the rough profiles by parabola functions obtained using simple parameters of roughness.

New contact equations are modified to match the revolution parabolic particle geometry in the present research. In the present contact models three deformation stages are totally considered. The load is calculated as a function of the interference of each profile for single parabolic asperities.

An expression of fitting curve for grooving ridge is got from the FEM computation for single particle in which the meanings of fitted constants are in accordance with that by Böklen's curves. At the same time, a new modified expression is proposed again based on the results of FEM calculation. By the FEM fitted curves. The effect of material hardness on ridge curve can be easily got by the interpretation operation.

The simulation is correspondingly operated under the same experimental conditions for three kinds of laboratory wear tests. The relationship between wear volume loss V and the Vickers hardness, for five specimens with different cementite contents is obtained. The wear volume loss decreases with increasing hardness under every simulated applied pressure. However, the wear rate which is simulated by computer is at about 50% less than the experimental value when Vickers hardness is higher than 800 HV. This is due to the fracture of cementite phase during real test with high volume fraction of cementite and applied pressure.

Worn surface profile at each individual step is also simulated. The simulated roughness Ra increases approximately linearly to 3.13 μm for the first 20 steps, then keeps up and down that value. In the experiment under the same conditions, the worn surface roughness for AISI1080 steel is measured to be equals Ra 3.22 μm. It can be seen that the final roughness of computer simulation progress exhibits slightly negative deviation and the relative error to experimental results is within 2.8%.

Acknowledgements

This research was supported by the National Natural Science Foundation of China through Grants No. 50475089. The present authors also gratefully acknowledges the financial support for attending the First ICAP in UK by K.C. Wong Education Foundation, Hong Kong, China. The roughness measurement of worn surface was carried out in the Institute of Tribology and Reliability Engineering, China University of Mining and Technology, Xuzhou, PR China. Thanks for their kind help to this research.

References

Abbott, E.J., Firestone, F.A., 1933. Specifying surface quality—a method based on accurate measurement and comparison. Mech. Eng. 55, 569–572.
Aramaki, H., Cheng, H.S., Chung, Y., 1993. The contact between rough surfaces with longitudinal texture: Part I. Average contact pressure and real contact area. ASME J. Tribol. 115, 419–424.
Azarkhin, A., Richmond, O., 1992. A model of ploughing by a pyramidal indenter: upper bound method for stress-free surface. Wear 157, 409–418.
Böklin, R., 1973. In: Westbrook, J.H., Conrad, H. (Eds.), The Science of Hardness Testing and its Research Applications. American Society for Metals, Metals Park, OH, pp. 109–247.
Ciulli, E., Ferreira, L.A., Pugliese, G., Tavares, S.M.O., 2008. Rough contacts between actual engineering surfaces: Part I. Simple models for roughness description. Wear 264, 1105–1115.
Fang, L., Cen, Q., Sun, K., Liu, W., Zhang, X., Huang, Z., 2005. FEM computation of groove ridge and Monte Carlo simulation in two-body abrasive wear. Wear 258, 265–274.
Greenwood, J.A., 2006. A simplified elliptic model of rough surface contact. Wear 261, 191–200.
Greenwood, J.A., Williamson, J.P.B., 1966. Contact of nominally flat surfaces. Proc. R. Soc. London Ser. 295 A, 300–319.
Hokirigawa, K., Kato, K., 1989. Theoretical estimation of abrasive wear resistance based on microscopic wear mechanism. In: Ludema, K.C. (Ed.), Proceedings of the International Conference on Wear of Materials, pp. 1–8.
Hokkirigawa, K., Kato, K., 1988. The effect of hardness on the transition of the abrasive wear mechanism of steels. Wear 123, 241–251.
Jacobson, S., Wallen, P., Hogmarkacobson, S., 1987. Fundamental aspects of abrasive wear studied by a new numerical simulation model. In: Ludema, K.C. (Ed.), Proceedings of the International Conference on Wear of Materials, pp. 595–606.
Jiang, J., Sheng, F., Ren, F., 1998. Modelling of two-body abrasive wear under multiple contact conditions. Wear 217, 35–45.
Johnson, K.L., 1985. Contact Mechanics. Cambridge Univ. Press, Cambridge, pp. 1–268.
Kayaba, T., Hokkirigawa, K., Kato, K., 1986. Analysis of the abrasive wear mechanism by successive observations of wear processes in a scanning electron microscope. Wear 110, 419–430.
M. M. Khruschov, Abrasion of Metals, Translated into Chinese by the Mechanical Industry Press, Beijing, 1966.
Nicholls, J.R., Stephenson, D.J., 1995. Monte Carlo modeling of erosion processes. Wear 186–187, 64–77.
Sasaki, T., Yakou, T., Umemoto, M., Todaka, Y., 2006. Two-body abrasive wear property of cementite. Wear 260, 1090–1095.
Tabor, D., 1951. The Hardness of Metals. Oxford University Press, Oxford, UK.
Tomanik, E., Chacon, H., Teixeira, G., 2003. A simple numerical procedure to calculate the input data of Greenwood–Williamson model of asperity contact for actual engineering surfaces. In: Leeds-Lyon Symposium on Tribology, Tribological Research and Design for Engineering Systems Tribology Series, 41. Elsevier, Amsterdam, pp. 205–216.
Umemoto, M., Todaka, Y., Takahashi, T., Li, P., Tokumiya, R., Tsuchiya, K., 2003. Characterization of bulk cementite produced by mechanical alloying and spark plasma sintering. Mater. Sci. Forum 15–16, 607–614.
Wu, G., Zhang, X., Fang, L., Xing, J., 2000. 3-D dynamic simulation of two-body abrasion. J. Xi'an Jiaotong Univ. 20 (5), 360–364.
Zhang, B., Xie, Y., 1989a. Two-body microcutting wear model: Part I. Two-dimensional roughness model. Wear 129, 37–48.
Zhang, B., Xie, Y., 1989b. Two-body microcutting wear model: Part II. Three-dimensional roughness model. Wear 129, 49–58.
Zhang, B., Xie, Y., 1989c. Two-body microcutting wear model: Part IV. Theoretical analysis of friction. Wear 129, 67–79.
Zhao, Y., Maietta, D.M., Chang, L., 2000. An asperity microcontact model incorporating the transition from elastic deformation to fully plastic flow. ASME J. Tribol. 122, 86–93.